Marine Micropaleontology 177 (2022) 102181

Contents lists available at ScienceDirect

Marine Micropaleontology

journal homepage: www.elsevier.com/locate/marmicro

The evolution of seafloor environmental conditions in the southern Red Sea continental shelf during the last 30 ka

S. Sergiou [a,*], M. Geraga [a], E.J. Rohling [b,c], L. Rodríguez-Sanz [b], A. Prandekou [a], A. Noti [a], F. Paraschos [a,d], D. Sakellariou [d], G. Bailey [e,f]

[a] Laboratory of Marine Geology and Physical Oceanography, Department of Geology, University of Patras, Patras 26504, Greece
[b] Research School of Earth Sciences, Australian National University, Canberra, ACT 2601, Australia
[c] Ocean and Earth Science, University of Southampton, National Oceanography Centre, Southampton SO14 3ZH, United Kingdom
[d] Institute of Oceanography, Hellenic Centre for Marine Research, 19013 Anavyssos, Greece
[e] Department of Archaeology, King's Manor, University of York, York YO1 7EP, United Kingdom
[f] College of Humanities, Arts and Social Sciences, Flinders University, Adelaide, SA 5001, Australia

ARTICLE INFO

Keywords:
Red Sea
Sea level changes
Seafloor conditions
Monsoon
Benthic foraminifera
Paleoceanography

ABSTRACT

The southern Red Sea is affected by intense interactions between monsoon and sea level changes in a semi-closed environment. Still, the impacts on the wide shelves remain poorly documented. We investigate the seafloor environmental conditions on the southern Red Sea shelf over the last 30 ka through sedimentological (visual inspection, granulometry, bulk density), geochemical (organic carbon, calcium carbonate and nitrogen content) and micropaleontological (benthic foraminifera) observations in a previously dated sediment core (FA09) from the Farasan Islands Archipelago. Glacial sediments exhibit high density and low carbonate contents, whereas post-glacial sediments reflect increased biogenic productivity. Seafloor oxygenation was limited in most of the glacial interval, along with hypersaline conditions. During the maximum sea level lowstand, an enhanced presence of eutrophic-indicator benthic assemblages likely reflects efficient organic matter preservation induced by weak water ventilation. Our proxies combined with a previous surface-water productivity reconstruction reveals a coupling between organic matter flux to the seafloor and surface productivity levels in the southern Red Sea shelf, particularly pronounced during periods of enhanced summer monsoon. This pattern is often accompanied by a decrease in seafloor oxygenation. In contrast, well oxygenated and more oligotrophic seafloor conditions are recorded around the time of Heinrich Stadial 2, when previous work indicates a reduction in summer monsoon intensity and surface productivity levels. A drastic decrease of benthic foraminifera along with increased organic carbon contents in late glacial and late Holocene reflect oxygen-depleted seafloor conditions that we attribute to expansion of an intensified southern Red Sea oxygen minimum zone (OMZ).

1. Introduction

Over the years, benthic foraminiferal population studies have become a fundamental tool for evaluating modern and past seafloor conditions. Benthic foraminiferal populations, diversity, microhabitats, and adaptive morphologies are affected by changes in depth, bottom water oxygen availability, and organic matter fluxes to the seafloor (Corliss and Fois, 1990; Barmawidjaja et al., 1992; Kaiho, 1994; Jorissen et al., 1995; Almogi-Labin et al., 1996; De Rijk et al., 1999a, 2000; Verma et al., 2021). In addition, bottom water conditions are strongly affected by sediment deposition processes. For instance, organic compounds associated with terrigenous input or sediment transport along the seabed slope influence both seawater productivity and the benthic substrate (Diz et al., 2004; Duros et al., 2017; Di Bella et al., 2021). Therefore, downcore examination of benthic foraminiferal assemblages in sediment records and comparison with sedimentological and geochemical parameters can provide valuable information on the paleoenvironmental history of a marine setting (Murray, 2006).

The southern Red Sea continental shelf (Fig. 1a, b) is characterized by intense bottom water changes over time in response to the combined impacts of the south Asian monsoon and sea level changes on the semi-closed geometry of the southern Red Sea margin (Siddall et al., 2004;

* Corresponding author.
E-mail address: sergiou@upatras.gr (S. Sergiou).

https://doi.org/10.1016/j.marmicro.2022.102181
Received 5 April 2022; Received in revised form 27 September 2022; Accepted 10 October 2022
Available online 18 October 2022

Bailey et al., 2015; Sakellariou et al., 2019; Sergiou et al., 2022). However, understanding is limited because only few studies have been undertaken.

Previous studies, focused in the deep Red Sea basin, have demonstrated the response of benthic foraminiferal assemblages to seawater environmental changes linked to Quaternary glacial-interglacial cycles (Locke and Thunell, 1988; Almogi-Labin et al., 1996; Badawi et al., 2005). Intense changes were found in seawater salinity and sea-floor eutrophication levels, which were associated with monsoon intensity variations (Badawi, 2015). Moreover, deep and bottom waters became highly saline during maximum glacial sea level lowstands due to severe restriction of the Red Sea connection with the open ocean (Locke and Thunell, 1988; Rohling et al., 1998), and occasional suboxic/anoxic bottom water conditions developed (Almogi-Labin et al., 1996). Benthic foraminiferal assemblages of the last 400 ka from the southern Red Sea basin show a prevalence of infaunal species (mainly *Bolivina variabilis,*

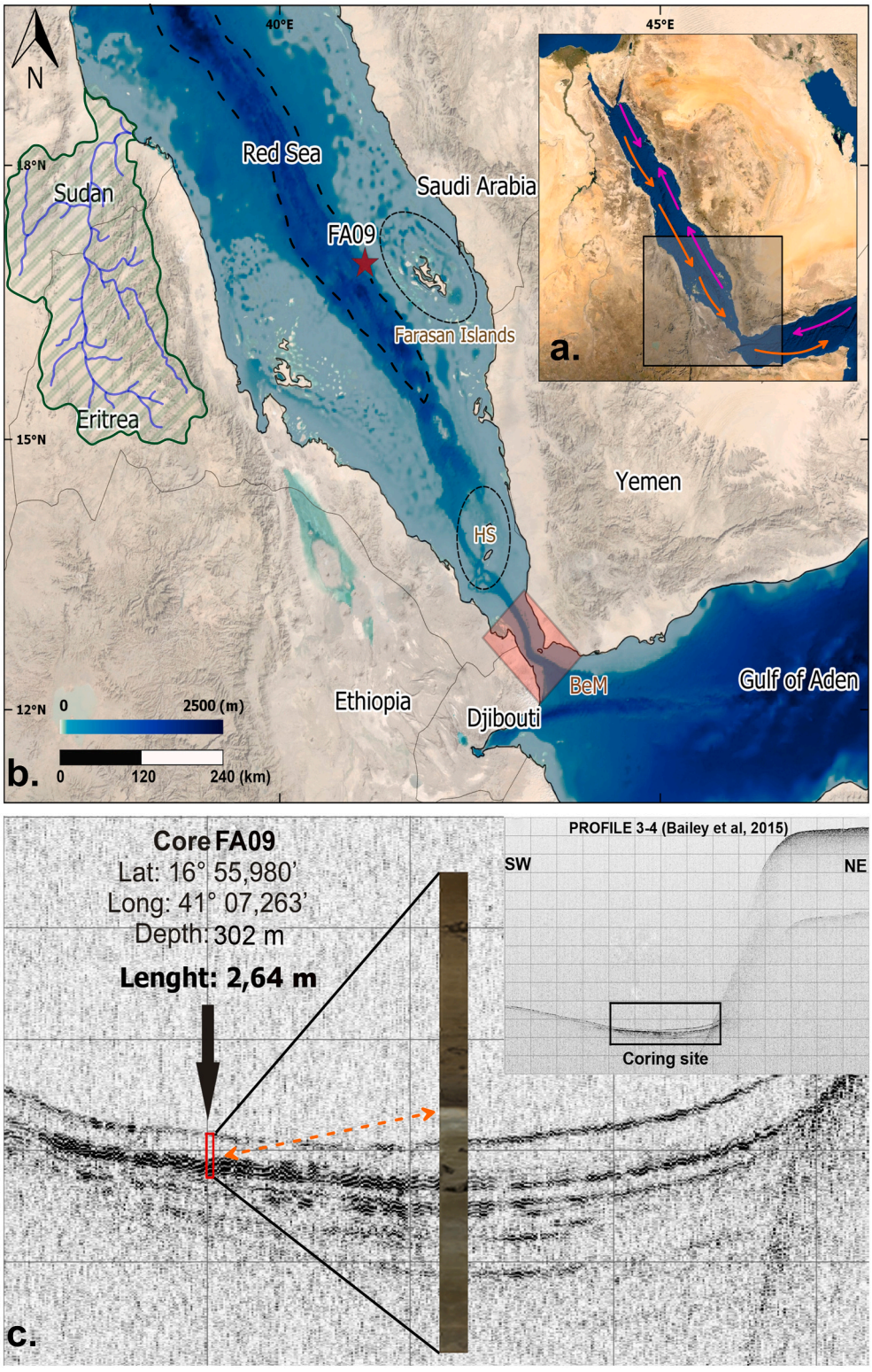

Fig. 1. (a) Monsoon driven circulation in the Red Sea basin. Winter (northeast) and summer (southwest) monsoon are indicated in purple and orange arrows respectively. **(b)** The southern Red Sea continental shelf bounded with dashed line. The Farasan Islands and Hanish Sill (HS) are indicated while the strait of Bab – el – Mandeb (BeM) is highlighted in red. The Baraka river catchment area is also depicted. **(c)** Seismic stratigraphy of the coring site and information of core FA09. Note the acoustic imprint of the major lithological differentiation at ~1.3 m below seafloor. For profile location, see Bailey et al. (2015) and Sakellariou et al. (2019). (For interpretation of the references to colour in this figure legend, the reader is referred to the web version of this article.)

Bulimina marginata, Uvigerina auberiana) and miliolid taxa during glacial intervals, which has been attributed to increased organic matter fluxes, low oxygen concentrations, and high salinity bottom water conditions (Badawi et al., 2005; Badawi, 2015). In contrast, dominance of epifaunal species (mainly *Cibicides mahabethi* and *Textularia* spp.) during interglacial intervals indicates well oxygenated bottom water conditions (Badawi et al., 2005; Badawi, 2015).

During the Holocene, when high sea level minimized restriction of the Red Sea from the open ocean (Siddall et al., 2003, 2004), benthic foraminiferal assemblages in the deep basin reflect variations in the bottom water oxygen content and surface productivity-driven organic matter fluxes to the seafloor; specific microfaunal associations appear to develop in accordance with changes in the extent of the Oxygen Minimum Zone (OMZ) (Edelman-Furstenberg et al., 2001). In nearshore and shallow Red Sea waters, benthic assemblages have also been used to assess the evolution of coastal semi-closed water bodies, tidal effects, coral reefs, and even anthropogenic impacts (Abou Ouf, 1992; Abou Ouf and El Shater, 1992; Basaham, 2009; Abu-Zied et al., 2011; Abu-Zied and Bantan, 2013; Bantan and Abu-Zied, 2014; Pavlopoulos et al., 2018; Abu-Zied and Orif, 2019).

Regarding the late Quaternary sedimentary history of the Red Sea, Mitchell et al. (2015) reported a strong correlation between sea level lowstands and increased Red Sea sediment bulk density, which can be linked with hypersaline conditions and increased heavy mineral contents including eolian components (Stoffers and Ross, 1974; Roberts et al., 2011), while Palchan et al. (2013) and Hartman et al. (2020) indicated eolian sediment provenance from both the Sahara and Arabia during glacial times based on isotopic, mineral, granulometric, and geochemical proxies. Additionally, the pioneering studies of Stoffers and Ross (1974) and Manheim (1974) noted a repeated presence of dark-coloured, organic rich intervals indicative of low oxygen bottom water conditions through the Quaternary sediment successions along the Red Sea basin. Later studies of Locke and Thunell (1988), Almogi-Labin et al. (1991) and Arz et al. (2003) distinguished the last appearance of these intervals near the late glacial to Holocene transition (lying between ca. 15–10 ka) in the central and northern Red Sea. These authors also discussed the relationships between sedimentary $CaCO_3$ and organic carbon contents during the last ~20 ka.

The present study aims to advance understanding of the impact of climate-driven processes on sea-floor conditions over the poorly explored southern Red Sea shelf region during the last 30 ka, using sediment core FA09 (Sergiou et al., 2022). For this, we examine the evolution of the seafloor environmental conditions through lithological (visual description, granulometry, bulk density), geochemical (organic carbon, calcium carbonate and nitrogen content) and micropaleontological (benthic foraminifera) observations. We interpret these new results within context of previous chronostratigraphic and surface water reconstructions for this site (Sergiou et al., 2022).

2. Study area: Geological and Oceanographic setting

The southern Red Sea is connected with the Indian Ocean through the 20-km wide straits of Bab el Mandeb (Fig. 1b). At the northern end of the straits lies the Hanish sill (137 m water depth), which marks the shallowest passage (Werner and Lange, 1975; Siddall et al., 2002; Biton et al., 2008; Lambeck et al., 2011).

Site FA09 is located within the bounds of the Farasan Islands Archipelago, Saudi Arabia (Fig. 1a, b). The Farasan Islands comprise predominately Pleistocene coral reef carbonates covered by recent coastal deposits enriched in various biogenic components (Bantan and Abu-Zied, 2014; Almalki and Bantan, 2016). Quaternary Red Sea sediments comprise principally hemipelagic carbonate oozes with varying contributions of eolian dust constituents (Stoffers and Ross, 1974; Roberts et al., 2011). On the southern shelf, carbonate rich sandy and muddy sediments cover the sea floor with mixed biogenic and terrigenous proportions (Abou Ouf and El Shater, 1992; Basaham, 2009). Riverine input is notable in southern parts of the Red Sea, relative to an absence in the rest of the basin (Rasul and Stewart, 2015). The Baraka River (Fig. 1b) is the most important ephemeral river in the region; it covers a catchment area of about 66 km^2, and is active most of the autumn season with an annual water discharge of 970 $\times$ 10^6 m^3 (Rasul and Stewart, 2015; Babker et al., 2020).

The oceanographic regime of the southern Red Sea is driven by seasonal monsoon changes (Fig. 1a). During winter (October–May), a two-layered system occurs with a relatively warm, low-salinity surface inflow from the Gulf of Aden (Gulf of Aden Surface Water-GASW) above a cooler, high salinity outflow that is present throughout the year (Red Sea Outflow Water-RSOW). This outflowing deep water mass originates in the northern Red Sea (Morcos, 1970; Woelk and Quadfasel, 1996; Sofianos and Johns, 2015). During summer (June–September), southern Red Sea hydrography consists of a three-layered system. A surficial layer of increased temperature and salinity exits the basin into the Gulf of Aden (Red Sea Surface Water-RSSW), above an intermediate inflow of nutrient-rich (upwelled) water from the Gulf of Aden (Gulf of Aden Intermediate Water-GAIW) (Sofianos and Johns, 2007, 2015; Dreano et al., 2016), and a continuing outflow of cooler, high salinity waters (RSOW). Dissolved oxygen concentrations in the upper water column (top 100 m) of the southern Red Sea range between 2 ml/l during winter (Woelk and Quadfasel, 1996) and 1.8–3 ml/l during summer (Sofianos and Johns, 2007). Oxygen concentrations decrease rapidly below 100 m, and an oxygen minimum zone (OMZ) occurs between 200 and 650 m water depth on an annual basis, with minimum oxygen concentrations of ~0.5 ml O_2/L in the southern Red Sea (Woelk and Quadfasel, 1996).

The southern Red Sea continental shelf experiences relatively productive conditions throughout the year due to the inflow of nutrient-enriched waters from the Gulf of Aden (Triantafyllou et al., 2014; Pearman et al., 2017; Li et al., 2018). Consequently, the shallow shelf environment is characterized by notable biological growth (Triantafyllou et al., 2014; Ellis et al., 2017).

3. Material and methods

3.1. Core sediments

Core FA09 (16.93°N, 41.12°E, 302 m water depth) was retrieved in summer 2013 as part of the DISPERSE project (Bailey et al., 2015, 2019). The core location was decided using high resolution seismic profiles (3.5 kHz) (Fig. 1c) (Bailey et al., 2015; Sakellariou et al., 2019). The core has a total length of 2.64 m and spans the last 30 ka (Sergiou et al., 2022).

Visual core description was conducted following the standards of Mazzulo and Graham (1988), focusing on variations of colour, texture, and sedimentary structures. Grain size analysis was performed using a Malvern Mastersizer 2000 particle analyzer on a total of 132 samples collected with downcore sampling spacing of 2 cm. Hydrogen peroxide (H_2O_2) treatment was applied prior to analysis to eliminate organic matter. Mean size (Mz) and sorting (σi) were calculated with the GRADISTAT software (Blott and Pye, 2001) while sediment classification follows Folk (1974) nomenclature. Dry bulk density (DBD) was determined with the gravimetric method (McNeill et al., 2019).

Total carbon (TC), total organic carbon (TOC) and total nitrogen (TN) contents were measured on 52 samples from key intervals along the core using a Carlo Erba EA1108 elemental analyzer. For TOC measurements, samples were treated with HCL (1 N) prior to analysis in order to remove inorganic carbonates, as suggested by Van Iperen and Helder (1985). The difference between TC and TOC contents is regarded as the total inorganic carbon (TIC) content. Subsequently, calcium carbonate percentages were calculated from TIC using: $CaCO_3$ (%) = (TIC) x 8.33 (Bunzel et al., 2017). TOC/TN ratios were calculated to distinguish between marine (values <10) and terrestrial (>10) organic matter sources (Meyers, 1994).

3.2. Benthic foraminiferal analysis

Benthic foraminifera were studied in 109 sediment samples, with a mean sample spacing of 2–3 cm (i.e., 230–340 years). Aliquots of dried and weighed sediment samples were used that contain over 200 specimens in the >125 μm size fraction. Specimens were counted and identified to species level (genus level in some cases) based on the World Register of Marine Species database taxonomy (WoRMS Editorial Board, 2021). Each taxon was quantified as number per gram (N/g) and as percentage (%) of the total benthic foraminiferal assemblage.

To assess variations in seafloor conditions, we grouped benthic foraminifera according to microhabitat preferences and morphotypes, which previous studies have linked to specific environments (Corliss and Fois, 1990; Jorissen et al., 1995, 2018; Verma et al., 2021). The main microhabitat distinction is between epifauna and infauna (Jorissen et al., 1995, 2018). Epifaunal taxa require higher seafloor oxygenation than infaunal taxa, which are more tolerant to decreased oxygen levels within the sediment (Barmawidjaja et al., 1992; Jorissen et al., 1995). Epifaunal taxa include rounded trochospiral, plano-convex trochospiral, biconvex trochospiral, and milioline morphotypes, while infaunal taxa include rounded planispiral, tapered or cylindrical, flattened tapered, spherical and flattened ovoid morphotypes (Corliss and Fois, 1990; Alperin et al., 2011; Verma et al., 2021). High relative abundances of infauna and/or tapered/cylindrical benthic foraminiferal tests are indicative of relatively poor seafloor oxygenation while high abundances of epifauna and/or plano-convex tests suggest well oxygenated seafloor conditions (Corliss and Fois, 1990; Kaiho, 1994; Alperin et al., 2011; Verma et al., 2021). Therefore, we present variations in the relative abundances of epifaunal and infaunal taxa (Epif. % – Inf. %) together with variations in the relative abundances of plano-convex and tapered/cylindrical morphological groups.

We also grouped benthic foraminiferal taxa into oxic, suboxic and dysoxic groups, in accordance to their responses to dissolved oxygen levels. Oxic group taxa require oxygen levels above 2 ml/l, suboxic group taxa can adapt to levels between 0.5 and 1.5 ml/l O_2, and dysoxic group taxa can tolerate very low oxygen concentrations (<0.5 ml/l) (Hermelin and Shimmield, 1990; Kaiho, 1994; Jannink et al., 1998; Singh et al., 2015; Verma et al., 2021).

Moreover, in order to evaluate the variations in seafloor organic enrichment, we clustered benthic foraminifera into two broad groups depending on their response to organic matter accumulation, based on Jorissen et al. (2018) and references therein. Our "oligotrophic" group includes taxa that avoid regions with organic enrichment (i.e., Ecological Group I: "sensitive species" of Jorissen et al., 2018). Our "eutrophic" group includes taxa with an affinity to organic enrichment, based on the sum of Ecological Goups II ("Indifferent species"), III ("Third-order

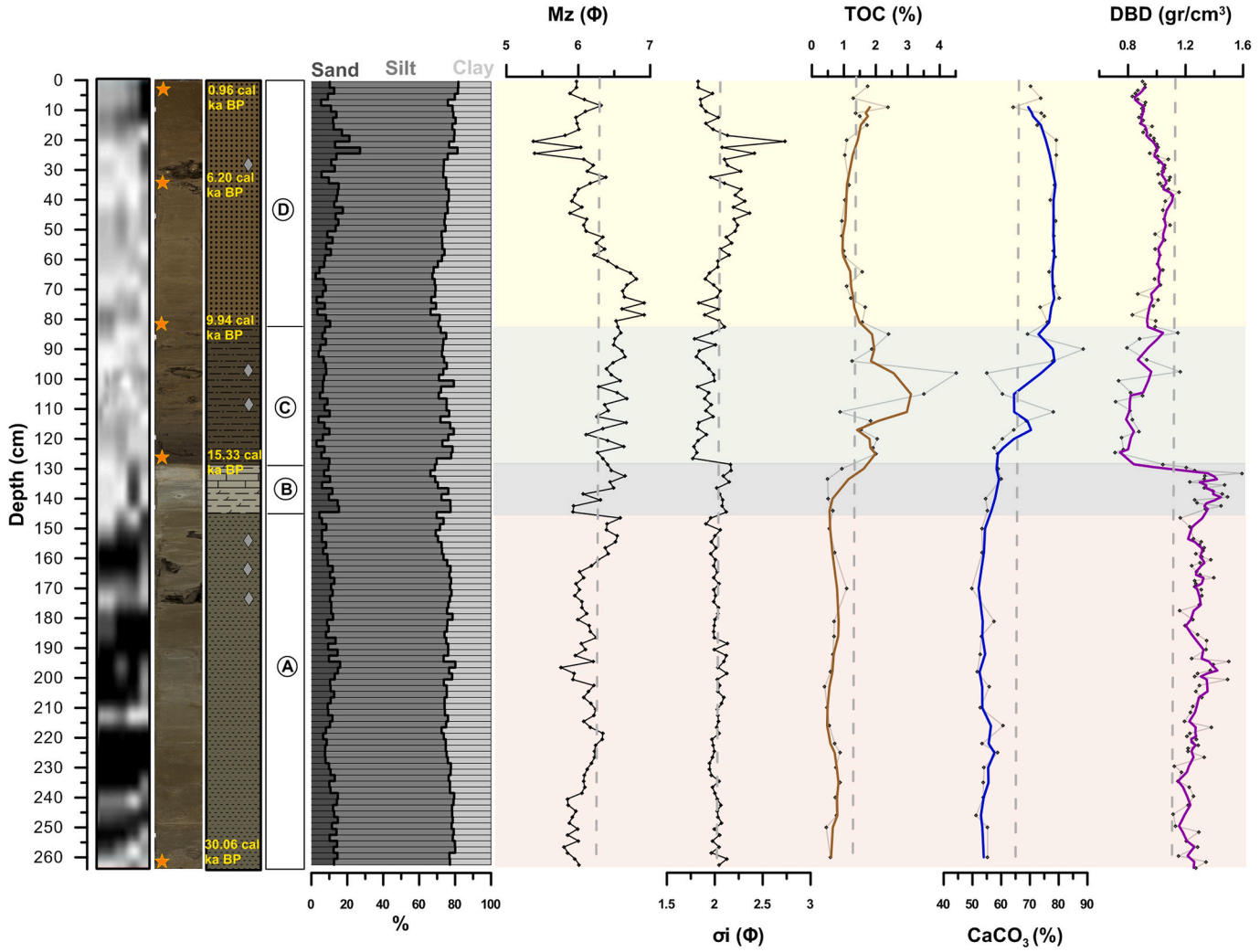

Fig. 2. Lithostratigraphy of core FA09. From left to right: Acoustic profile, core photo and illustration, lithological units and downcore variation of grain size, statistical parameters (mean, sorting), TOC, $CaCO_3$ and Dry Bulk Density (DBD). Calibrated radiocarbon dates (orange stars) are obtained from Sergiou et al., 2022. Intraclasts are indicated in gray diamond shapes.

opportunists"), IV ("Second-order opportunists"), and V ("First-order opportunists") of Jorissen et al. (2018). Thus, we view the ratio of the eutrophic versus oligotrophic groups in FA09 core as an indicator of organic matter export to the seafloor.

Finally, we classified the benthic foraminiferal taxa according to their wall-structure type in Hyaline, Agglutinated and Porcelaneous groups and evaluated their downcore participation. The relative abundance between these three groups reflects important information on the dominant seafloor environmental conditions, mostly related to salinity, trophic state and depth gradients (Murray, 2006).

All data for benthic foraminifera taxa and groups for core FA09 are given in supplementary file SF1.

4. Results

4.1. Lithostratigraphy

FA09 comprises fine-grained, poorly to very poorly sorted sediments with occasional presence of lithic and coral intraclasts (Fig. 2). There are four Lithological Units (LU A to LU D), which according to the core chronology (Sergiou et al., 2022) correspond to specific climatic periods (Table 1).

Silt is the dominant size fraction throughout. Relative proportions of sand and clay suggest an upward fining trend though LU A and LU B, and an upward coarsening trend in LU D (Fig. 2). $CaCO_3$ content is low, and dry bulk density (DBD) is high in the glacial sediments (LU A and LU B). In contrast, $CaCO_3$ content is high and DBD is low in the late glacial (LU C) and Holocene (LU D) intervals. High DBD between 129 and 264 cm explains the high amplitude reflections in the seismic profile from the coring site (Fig. 2). Mean TOC values are ~1.2% throughout the core. Maximum TOC values (>1.5%) occur throughout the late glacial interval (LU C), while minor increases are recorded within LU A (around 222–246 cm and 160–185 cm) and near the core top (LU D) at around 9–17 cm.

4.2. Benthic foraminifera

Benthic foraminifera are variably present in all examined samples; abundances are high throughout the core, except in LU C and the top of the LU D (Fig. 3a). In total, 99 benthic foraminiferal species have been identified, with *Bolivina, Bulimina, Cibicides, Anomalinoides, Hanzawaia, Quinqueloculina, Reophax, Cibicidoides*, and *Uvigerina* as the dominant genera.

Downcore abundance variations of the dominant benthic foraminiferal genera/ species are shown in Fig. 3. Each taxon shows notable variations, including intervals of absence. *Bolivina* is represented by *B. alata, B. dilatata, B. limbata, B. persiensis, B. spathulata, B. subaenariensis,* and *B. variabilis.* Bolivinid abundances are enhanced in the glacial section (LU A and LU B) (Fig. 3b), with relatively low numbers at around 145–172 cm and 190–217 cm. At around 145–172 cm, bolivinids are replaced by a maximum occurrence of buliminids. Buliminids are represented mainly by *B. marginata* and *B. elongata* (Fig. 3c). Bolivinids and buliminids present concurrent variations in the post-glacial sediments (LU C and LU D), and both show high abundances at the onset of the early Holocene (base of LU D) that contrast with relatively low numbers in the late glacial period and the rest of the Holocene. Buliminids and bolivinids mainly occur in benthic assemblages of organic-rich environments while many of them tolerate low oxygen levels (Sen Gupta and Machain-Castillo, 1993; Kaiho, 1994; Mendes et al., 2004; Murray, 2006; Abu-Zied et al., 2008). Accordingly, the specific buliminid and bolivinid species of the FA09 core are typical indicators of eutrophic and dysoxic seafloor conditions (see supplementary file SF1). Uvigerinids are also known to prefer enhanced organic flux to the seafloor and tolerate dysoxia, although their low O_2 tolerance is less developed than that of bolivinids and buliminids (Sen Gupta and Machain-Castillo, 1993; Kaiho, 1994). In FA09, uvigerinids are represented by *Uvigerina peregrina* and *Neouvigerina porrecta*, with high abundances towards the base of the core (218–264 cm; Fig. 3d). Minor contributions of uvigerinids are recorded near the base of LU C (onset of the late glacial period) and around 20–60 cm (middle Holocene).

The miliolids mainly include *Quinqueloculina, Miliolinella, Spiroloculina, Sigmoilopsis, Spirophthalmidium, Triloculina*, and *Massilina* (in decreasing order of abundance). Miliolids are associated with oxic and oligotrophic environments (Platon et al., 2005; Murray, 2006). In addition, miliolids have been recorded in high numbers during the development of high salinity conditions in the Red Sea (Locke and Thunell, 1988; Rohling et al., 1998; Badawi et al., 2005). Agglutinant taxa are also common in high salinity shelf environments (Sen Gupta, 2003; Abu-Zied et al., 2011; Abu-Zied and Bantan, 2013). In FA09, agglutinants mainly include *Reophax, Textularia*, and *Haddonia*. Both the miliolid and agglutinant groups are more abundant in glacial sections (LU A and LU B) than in post-glacial sections (Fig. 3e, f). Miliolid and agglutinant abundance variations covary throughout the glacial period except between 225 and 240 cm, where only the abundance of agglutinants is elevated.

Throughout FA09, epifauna is dominated by the *Cibicides* group (represented mainly by *C. mabahethi* and *C. refulgens*), along with *Cibicidoides mundulus, Anomalinoides colligera,* and *Hanzawaia* sp. (Fig. 3g-j). Abundances of these taxa covary throughout the core, with high values at 170–217 cm, at the end of the glacial period (LU B), and at 28–80 cm (the early and middle Holocene). These taxa prefer well oxygenated bottom water conditions (Kaiho, 1994; Badawi et al., 2005; Murray, 2006).

The downcore percentage variation of the dominant benthic species identified in core FA09 is presented in supplementary file SF2.

Table 1
Identified Lithological Units in core FA09. Age ranges derived using the chronological framework of Sergiou et al. (2022).

Lithological Units	Depth (cm)	Age range (ka)*	Climatic Period	Characteristics
LU A	264–144	ca. 30–17	*Glacial*	*Light brownish gray (2.5Y 6/2) poorly sorted sandy silt*
LU B	144–129	ca. 17–15	*Glacial, Heinrich stadial 1 (HS1)*	*Light gray (2.5Y 7/1) to white (2.5Y 8/1) very poorly sorted sandy silt*
LU C	129–84	ca. 15–10.5	*Late Glacial*	*Organic-rich, weakly laminated, very dark grayish brown (2.5Y 3/2) to olive brown (2.5Y 4/3) poorly sorted silt*
LU D	84–0	ca. 10.5–0	*Holocene*	*Carbonate-rich light olive brown (2.5Y 5/4) poorly to very poorly sorted sandy silt*

5. Discussion

5.1. Imprints of glacial and post-glacial conditions in the sediment texture

The end of the glacial period is well defined in FA09 by a sharp, abrupt contact between LU B and LU C, along with a major colour switch, which implies a drastic environmental transition at ~15 ka (Fig. 2). This is supported by a clear differentiation between glacial (30–15 ka) and post–glacial (last 15 ka) conditions in most proxies. Most pronounced is an inverse correlation between density and carbonate content (Fig. 4a, b). A similar pattern has been observed in core KL11 from the central Red Sea; Mitchell et al. (2015) reported that during Quaternary climate cycles, densities (carbonate contents) were high (low) during glacial sea level lowstands, whereas the opposite applies to sea level highstands. The high glacial densities were attributed (to a

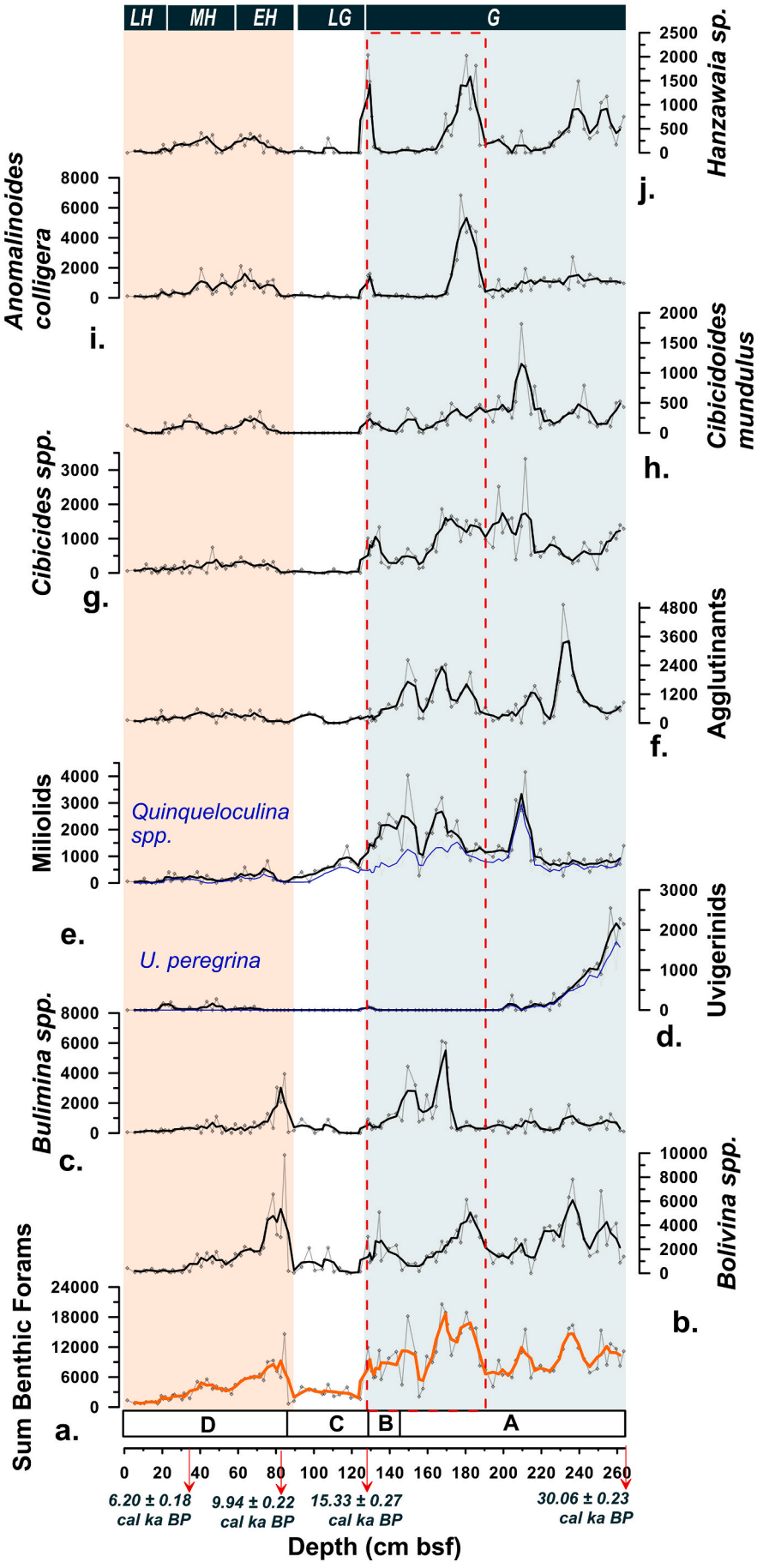

Fig. 3. Downcore distribution (specimen/g; N/g) of **(a)** the total benthic foraminiferal assemblages and **(b-j)** the dominant taxa and groups. The 130–190 cm interval (dashed rectangle) corresponds to the shallowest water depth formation in the coring site (see text). The Lithological Units (LU A-D) and the calibrated ages are shown in the lower section. The upper horizontal bars stand for the glacial (G), late glacial (LG), early Holocene (EH), middle Holocene (MH) and late Holocene (LH) chronostratigraphic intervals; derived from the chronological framework of Sergiou et al. (2022).

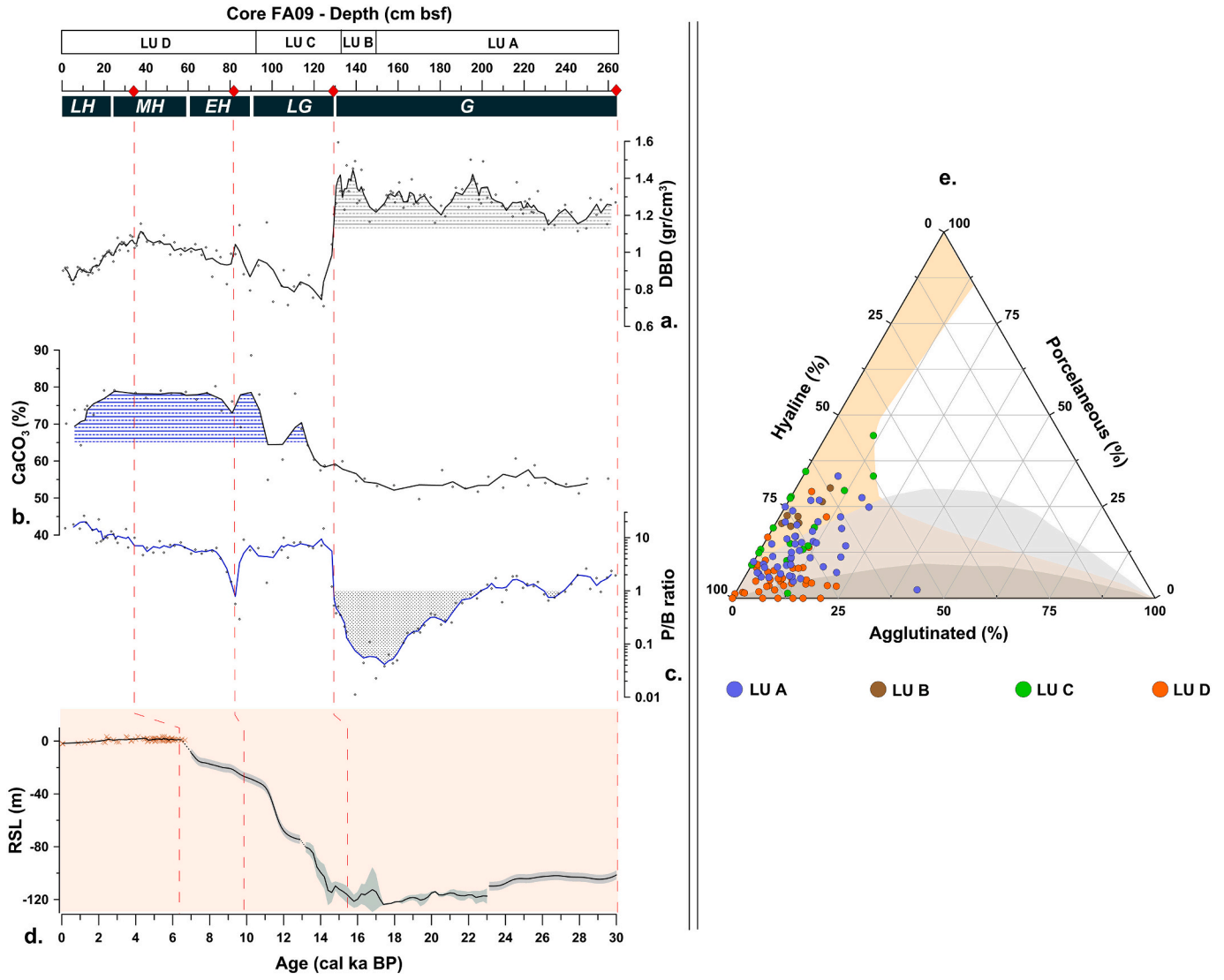

Fig. 4. (a-c) Glacial-Interglacial shifts in the FA09 records. P/B ratio values in (c) are presented in exponential scale. Lithological Units and chronostratigraphic intervals as in Fig. 3. **(d)** Relative sea level (RSL) reconstruction after combining the curves of Grant et al. (2012) (gray shaded - bands) with Arz et al. (2007) (23–13 ka; green shaded – bands curve) and the coastal sea level markers of Al-Mikhlafi et al. (2021) for the last 7 ka. **(e)** Ternary plot of the benthic foraminifera assemblages in FA09 based on wall-structure morphotypes (Murray, 2006). Marginal and shelf hypersaline environments are indicated by orange and light-gray shades respectively. Dark-gray area corresponds to deep-sea environment. (For interpretation of the references to colour in this figure legend, the reader is referred to the web version of this article.)

large extent) to the high eolian input that includes heavy minerals from the Sahara and Arabian domains, together with the decrease of biogenic carbonate due to high salinity in the Red Sea (Locke and Thunell, 1988; Arz et al., 2003; Roberts et al., 2011; Palchan et al., 2013). The drastic calcium carbonate increase in Red Sea sediments through the deglaciation and Holocene reflects a major improvement of biogenic productivity as sea level rose and interaction with the Gulf of Aden was restored, which alleviated the ecosystem impacts of extreme glacial salinity (Almogi-Labin et al., 1991; Fenton et al., 2000; Trommer et al., 2010; Sergiou et al., 2022). Extensive erosion of the reef platforms surrounding the Farasan Islands (Pavlopoulos et al., 2018) may also have contributed to the high Holocene carbonate values in FA09; as is observed today (Abou Ouf and El Shater, 1992; Basaham, 2009).

The glacial-interglacial DBD variation is visible also in the seismic stratigraphy at the core location. Enhanced acoustic reflection marks the glacial (high DBD) section, while the (low DBD) post-glacial sediments are acoustically transparent (Figs. 1c, 2). A similar contrast has been observed in seismic profiles from the central Red Sea (Mitchell et al., 2015). This indicates consistent sediment density changes throughout (at least) the southern and central Red Sea during the Quaternary.

5.2. *Benthic foraminiferal impacts of glacial and post-glacial sea level changes*

Red Sea benthic foraminiferal assemblages also reflect the glacial-interglacial shift. During the Quaternary, benthic foraminiferal distributions in the Red Sea were controlled by: (a) sea level and associated salinity fluctuations (Locke and Thunell, 1988; Almogi-Labin et al., 1996; Rohling et al., 1998; Badawi, 2015), (b) organic matter export fluxes to the seafloor (Almogi-Labin et al., 1996; Edelman-Furstenberg et al., 2001; Badawi et al., 2005; Abu-Zied, 2013), and (c) seafloor oxygenation as related to circulation and the OMZ extent (Edelman-Furstenberg et al., 2001; Badawi et al., 2005).

The ratio of planktic versus benthic foraminiferal abundances (P/B ratio) has long been used as a rough indication of water depth (Van der Zwaan et al., 1990; De Rijk et al., 1999b; Herkat and Ladjal, 2013). The P/B ratio in FA09 (302 m water depth) follows the sea level progression (Fig. 4c, d) (Arz et al., 2007; Grant et al., 2012; Al-Mikhlafi et al., 2021),

with dominance of benthic over planktic species during glacial times, and a maximum benthic dominance at 130–190 cm (~22–15 ka), which most likely corresponds to the maximum lowstand (Fig. 4d). This is consistent with a glacial sea-level lowering of ~120–130 m at the maximum lowstand, which would have reduced the water depth over the core location from ~300 m to ~170 m. The sea-level imprint on the P/B ratio is supported by the benthic foraminiferal wall structure type clustering (Murray, 2006) of LU A, LU B and LU C samples (glacial and late glacial) in the fields of marginal and shelf hypersaline environments, versus clustering of LU D (Holocene) samples in the hypersaline deep sea field (Fig. 4e).

High abundances of miliolids and agglutinants occur in the glacial sections (LU A and B), together with bolivinids, buliminids and uvigerinids (Fig. 3). As presented in supplementary file SF2, *Quinqueloculina* species (*Q. bosciana, Q. lamarckiana*), *Reophax* sp., *Bolivina variabilis, Bulimina marginata* and *Uvigerina peregrina* are the dominant species in most of these sediments. High abundances of *B. variabilis, B. marginata* and *U. peregrina* are indicative of oxygen-depleted seafloor conditions (Sen Gupta and Machain-Castillo, 1993; Kaiho, 1994; Sen Gupta, 2003; Murray, 2006), while miliolids and agglutinants are indicative of hypersaline conditions in the present Red Sea (Abu-Zied et al., 2011) and during glacials (Locke and Thunell, 1988; Badawi et al., 2005). Thus, the benthic assemblages in FA09 suggest establishment of low oxygen, high salinity seafloor conditions in relatively shallow waters for most of the glacial interval.

Finally, the presence of both planktic foraminifera (in low abundance; Sergiou et al., 2022) and benthic foraminifera (this study) in FA09 during the maximum sea level lowstand suggests a continuous marine influence at the Farasan Archipelago, which in turn indicates that water-exchange through the Bab el Mandeb strait remained active, albeit seriously restricted. This agrees with previous studies, which suggest limited but ongoing connection of the Red Sea with the open ocean during glacial times (Rohling and Zachariasse, 1996; Rohling et al., 1998; Fenton et al., 2000; Arz et al., 2003; Siddall et al., 2003; Fernandes et al., 2006).

5.3. Other paleoclimatic effects imprinted on the benthic foraminiferal assemblages

We evaluate seafloor environmental conditions using the abundance variations of benthic foraminiferal groups based on microhabitat preferences and morphotypes (Figs. 5, 6), along with independent proxies based on the TOC content, the TOC/TN ratio, and the sum of more eutrophic planktic foraminiferal species in FA09 (i.e., the Paleo-Productivity (PP) curve of Sergiou et al., 2022) (Fig. 5b, c, d). We emphasize that the term eutrophic is used here in a relative sense for the Red Sea, which is a highly oligotrophic region in general.

High eutrophic benthic foraminiferal abundances coincide with high eutrophic planktic foraminiferal numbers, which suggests a direct coupling between surface productivity and organic matter fluxes to the seafloor at the site of FA09 (Fig. 5a, b). This is observed especially at two short glacial intervals (around 217–236 cm and 169–175 cm), the late glacial-early Holocene period (80–110 cm) and during the late Holocene (9–28 cm). These relatively eutrophic intervals also contain low (high) relative abundances of oxic (dysoxic) and plano-convex (tapered/cylindrical) benthic foraminiferal taxa that indicate reduced oxygen concentrations on the seafloor (Fig. 6b, c). The association with low oxygen indicators is less obvious at 169–175 cm and 9–28 cm (late Holocene), which suggests that oxygen reductions on the seafloor did not depend exclusively on enhanced organic matter fluxes; i.e., circulation-driven changes in oxygen advection onto the shelf played a role as well.

Today, inflow of nutrient-enriched water masses from the Arabian Sea and the Gulf of Aden causes elevated productivity levels in the southern Red Sea, relative to low levels in the central and northern

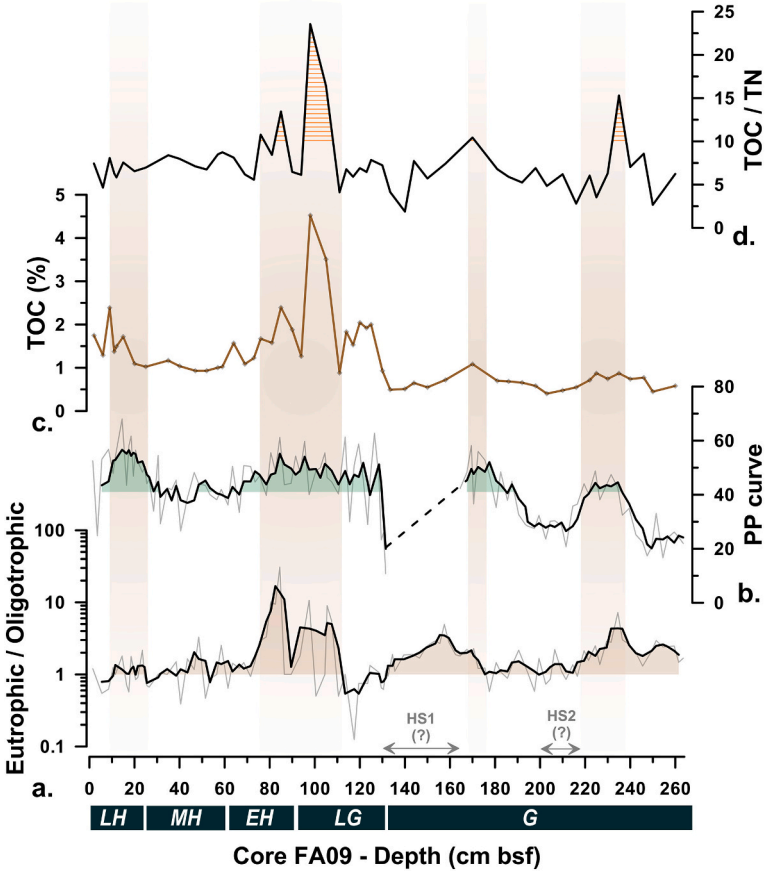

Fig. 5. Downcore variation of **(a)** eutrophic vs. oligotrophic indicator species along with **(b)** the surface paleoproductivity (PP) curve of Sergiou et al., 2022, **(c)** TOC content and **(d)** TOC/TN ratio in FA09 core. Note the intervals of concurrent increase of TOC, surface water and seafloor eutrophication. In the TOC/TN ratio, values higher than 10 suggest terrestrial origin of organic matter (Meyers, 1994). Chronostratigraphic intervals as in Fig. 3. The 200–215 cm and 130–164 cm intervals potentially correspond to the Heinrich Stadials (HS) 2 and 1.

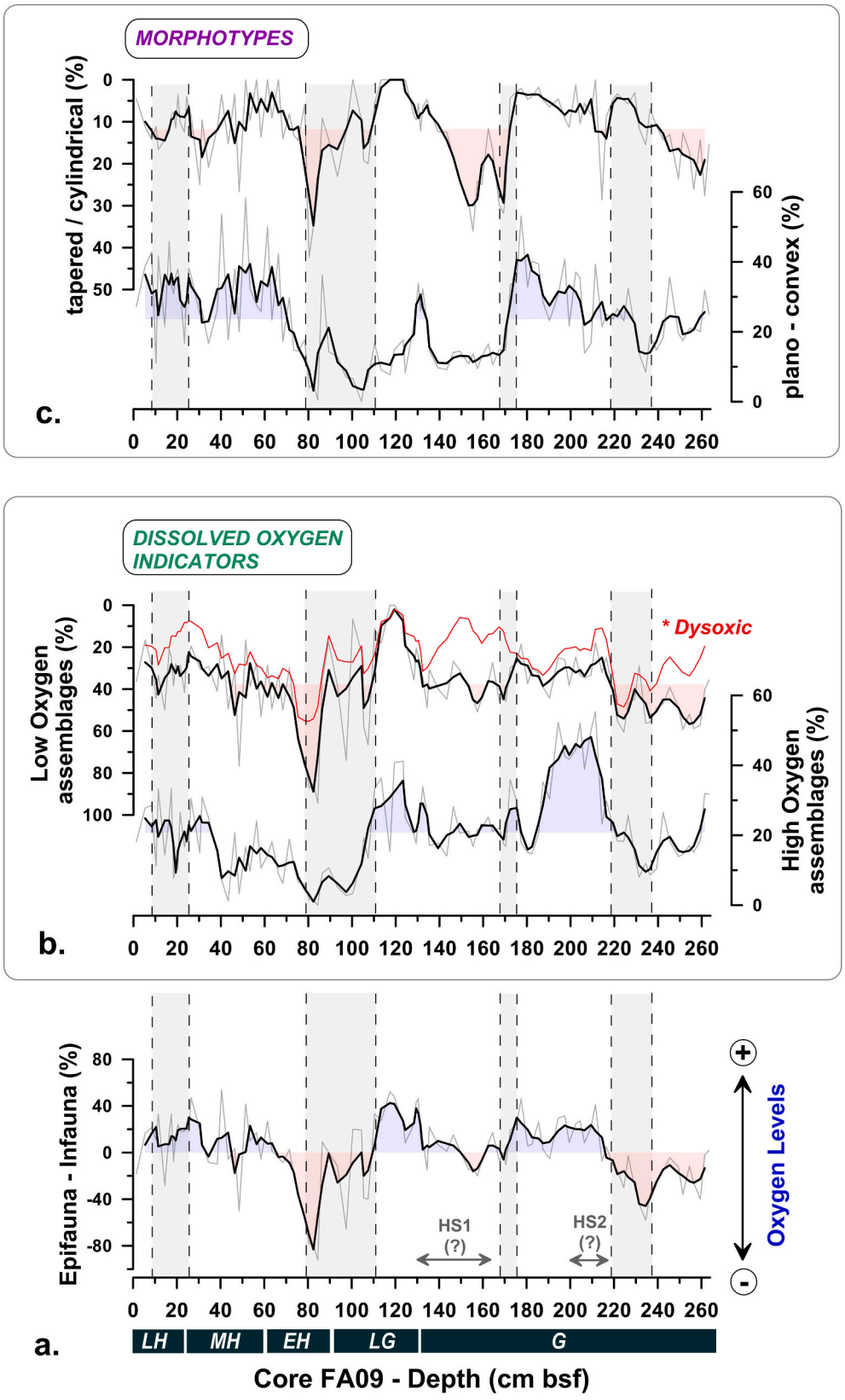

Fig. 6. **(a)** Relative abundance of epifaunal and infaunal benthic foraminiferal assemblages along the FA09 core. **(b, c)** Downcore distribution of the dissolved oxygen levels indicators and the main morphotype groups. Intervals with dominant blue-shaded value ranges correspond to well oxygenated seafloor conditions whereas intervals of red-shaded ranges indicate rather low oxygen levels. The intervals of surface productivity - seafloor organic matter fluxes coupling (Fig. 5) are indicated in light gray shades. (For interpretation of the references to colour in this figure legend, the reader is referred to the web version of this article.)

sectors (Triantafyllou et al., 2014; Raitsos et al., 2015; Dreano et al., 2016; Pearman et al., 2016). Summer monsoon winds favor upwelling that enriches nutrients in the northwestern Arabian Sea (Anderson and Prell, 1992; McCreary et al., 1996; Gittings et al., 2017), and orbital (precession) cycles cause alternation between periods with more intense summer monsoons and periods with weaker summer monsoons (Leuschner and Sirocko, 2000; Clemens and Prell, 2003; Caley et al., 2011; Böll et al., 2015; Gaye et al., 2018). Within the examined period, a major strengthening of the summer monsoon has been reported for the late glacial and early Holocene periods (Ivanochko et al., 2005; Shakun

et al., 2007; Gaye et al., 2018), while temporarily increased summer monsoons may have occurred also at times during the glacial interval (ca. 30–15 ka) (Naidu and Malmgren, 1996; Schulz et al., 2002; Singh et al., 2016; Sergiou et al., 2022). Extended upwelling of nutrient-rich waters in the northwestern Arabian Sea and the Gulf of Aden (Ivanochko et al., 2005; Gaye et al., 2018) during times with intensified summer monsoons would promote inflow of more nutrient-rich waters into the Red Sea, driving enhanced surface productivity in the southern Red Sea (Siccha et al., 2009; Sergiou et al., 2022). Meanwhile, increased precipitation associated with enhanced monsoon circulation may increase terrestrial organic matter input in the water column (similar to enhanced Baraka river input plain during the last interglacial monsoon maximum; Trommer et al., 2011). Therefore, elevated eutrophic species numbers both on the surface and at the seafloor, together with increased TOC contents and strong TOC/TN ratio fluctuations, in both the late glacial/early Holocene and two short glacial intervals (217–236 cm and 169–175 cm) (Fig. 5), suggest a combination of marine productivity-driven and terrigenous-driven organic matter fluxes to the seafloor at the coring site during intensified summer monsoon periods.

This signal is strongest in the late glacial-early Holocene (between ca. 13–9 ka based on linear sedimentation rate estimates; Sergiou et al., 2022), when the TOC content is high and TOC/TN values suggest major alternations between marine and terrestrial carbon sources (Fig. 5c, d). In addition, a severe reduction in benthic population density during most of that time (Fig. 3a) indicates a prevalence of highly stressed bottom water conditions due to a combination of enhanced biological oxygen demand and reduced advective oxygen supply. This suggests the presence of a stratified water column with a productive mixed layer and advection of low oxygen deeper waters onto the shelf. A similar pattern has been recognized in the central Red Sea at that time (Almogi-Labin et al., 1991). In addition, the preservation of depositional laminations in LU C sediments (Table 1) suggests decreased levels of bioturbation in an oxygen-depleted bottom water environment (Schimmelmann et al., 2016). At about the same period, benthic foraminifera decline in the deep southern Red Sea (Badawi et al., 2005) and the Gulf of Aden (Almogi-Labin et al., 2000), which implies the development of low-oxygen stress in deep water throughout the wider area. During the late glacial, elevated TOC contents in sediments from the north/northwestern Arabian Sea (Schulz et al., 1998; Ivanochko et al., 2005; Deplazes et al., 2014) and the Gulf of Aden (Locke and Thunell, 1988; Fersi et al., 2016) suggest increased productivity in the wider region. The combination of enhanced surface productivity and low oxygen deep waters has been related to a well-structured, extended OMZ in the northwestern Arabian Sea (Reichart et al., 1998; Gaye et al., 2018) under a dominant summer monsoon circulation pattern. We infer that during the late glacial and early Holocene, the seafloor of the southern Red Sea continental shelf experienced the influence of an intensified OMZ, driven by interaction with water masses of the Gulf of Aden and northwestern Arabian Sea, and exacerbated by local processes.

Millennial-scale cold intervals such as the Heinrich stadials (HS; Sanchez-Goni and Harrison, 2010) have been associated with decreased summer monsoon intensities (Leuschner and Sirocko, 2000; Ivanochko et al., 2005; Deplazes et al., 2014; Lauterbach et al., 2020). Increased aridity and reduced marine productivity prevailed in the Arabian Sea region (Ivanochko et al., 2005; Singh et al., 2011; Deplazes et al., 2014). Consequently, inflow into the southern Red Sea would have been relatively nutrient poor. This may explain the low surface productivity levels at 200–215 cm and 130–164 cm in FA09 which seem to coincide with HS2 (26.5–24.3 ka) and HS1 (18–15.6 ka), respectively (Sergiou et al., 2022) (Fig. 5). Regarding the 200–215 cm interval, concurrent high (low) relative abundances of oxic (dysoxic) and plano-convex (tapered/cylindrical) benthic foraminifera, together with high (low) abundances of oligotrophic (eutrophic) taxa, reflect limited organic matter export to the seafloor, and a prevalence of well oxygenated and oligotrophic seafloor conditions (Figs. 5a, 6). However, the benthic foraminiferal associations of FA09 suggest eutrophic and low oxygen seafloor conditions for the 130–164 cm interval (Figs. 5a, 6). This suggests that low sea level (Fig. 4d) and decreased monsoon intensity during HS1 caused a restricted water circulation pattern leading to decreased ventilation of the water column and, consequently, suboxic-dysoxic seafloor conditions in the shallow shelf of the southern Red Sea, favoring organic matter accumulation despite limited organic matter supply (i.e., preservation dominated accumulation).

During the late Holocene (9–28 cm in FA09), increased eutrophication at the coring site is linked with increased primary productivity along the southern and central Red Sea (Fig. 5a, b), although this was not associated with summer monsoon intensification (Edelman-Furstenberg et al., 2009; Siccha et al., 2009; Sergiou et al., 2022). However, the development of relatively eutrophic and oxygen-poor conditions, as recorded by benthic foraminifera and the TOC content (Fig. 5a, c; 6b), may be related to the extent of the OMZ and increased stratification of the water column. The OMZ developed between 200 and 650 m water depth since ~6 ka (Edelman-Furstenberg et al., 2001), following stabilization of sea level (Fig. 4d). It thus became an important influence on the FA09 core site (302 m depth), leading to enhanced organic matter preservation on the seafloor. Earlier in the Holocene (~9–6 ka), concurrently high numbers of *Bolivina* spp. and epifaunal, oligotrophic taxa (*Anomalinoides colligera*, *Cibicides* spp., *Hanzawaia* sp.) (Fig. 3 and supplementary file SF2) likely imply high-frequency fluctuations in organic matter fluxes and/or bottom water ventilation (Edelman-Furstenberg et al., 2001; Badawi et al., 2005; Murray, 2006), so that a highly unstable OMZ is inferred.

The drastic drop in benthic foraminiferal numbers over the last 6 ka (Fig. 3a) further supports the concept of an intensified OMZ affecting the southern Red Sea seafloor. However, reduction of the benthic population could also be the outcome of dilution effects provoked by increased terrigenous input (Saraswat et al., 2018). In fact, intense erosion of the reefal platforms surrounding Farasan islands has been suggested for the last 6 ka (Pavlopoulos et al., 2018). These processes could lead to high accumulation of near-source, coarse grained material at the outer shelf leading to increased participation of sand-sized sediments in the coring site (Fig. 2). Terrigenous matter dilution might have also contributed in the benthic fauna reduction discussed earlier for the late glacial interval, driven by enhanced monsoonal runoff (depicted in the high TOC/TN values; Fig. 5d).

6. Conclusions

The association between sediment properties and seafloor environmental conditions on the southern Red Sea continental shelf over the last 30 ka has been investigated using lithological, geochemical, and micropaleontological (benthic foraminifera) proxies in a sediment core from 302 m water depth in the Farasan Islands Archipelago. Results show that the transition from the last glacial period to the Holocene was marked by a notable drop in sediment density and increase in carbonate and TOC contents that suggests an overall improvement in biogenic productivity with sea level rise.

Benthic foraminiferal assemblages suggest that, during the glacial period (ca. 30–15 ka), low oxygen and high salinity seafloor conditions were established in a relatively shallow environment. During the maximum sea level lowstand (~22–15 ka) this led to organic-rich seafloor conditions, reflecting efficient preservation of the organic matter in the oxygen-depleted sediments.

The comparison of our geochemical and benthic faunal proxies with a previous surface-water productivity reconstruction reveals four intervals of strong coupling between organic matter flux on the seafloor and surface productivity levels in the southern Red Sea shelf: two brief ones during the glacial period, and two post-glacial ones corresponding to the late glacial-early Holocene (maximized between ~13–9 ka) and the late Holocene (last ~6 ka). The older three of these intervals coincide with periods of enhanced summer monsoon intensity and comprise organic matter sources that are both marine productivity-driven and

terrigenous input-driven, which implies influences both of nutrient-enriched inflow from the Gulf of Aden and increased riverine runoff. In contrast, oligotrophic seafloor conditions are observed at around Heinrich Stadial 2 (HS2), associated with a previously documented reduction in summer monsoon intensity and surface productivity levels.

Pronounced reduction in benthic foraminiferal abundances occurred during the late glacial (~15–11 ka) and late Holocene (last ~6 ka), associated with low-oxygen seafloor conditions. In both cases, the faunal decrease seems linked with an intensified oxygen minimum zone (OMZ) under well stratified water column conditions in the southern Red Sea, which we infer expanded onto the shelf region.

Declaration of Competing Interest

The authors declare that they have no known competing financial interests or personal relationships that could have appeared to influence the work reported in this paper.

Data availability

Data will be made available on request.

Acknowledgments

The present study arises from the “DISPERSE: Dynamic Landscapes, Coastal Environments and Human Dispersals” research project, funded by the European Research Council under the Ideas Programme of the 7th Framework Programme as Advanced Grant 269586. We thank the Saudi Commission for Tourism and National Heritage (SCTH) and the Department of General Survey of the Ministry of Defense for fieldwork permissions. We are also grateful to the crew of the R/V AEGAEO for successfully undertaking the coring survey. Finally, S. Sergiou thanks the General Secretariat for Research and Technology (GSRT) and the Hellenic Foundation for Research and Innovation (HFRI) for scholarship funding during his research work. This is DISPERSE contribution no. 65.

Appendix A. Supplementary data

Supplementary data to this article can be found online at https://doi.org/10.1016/j.marmicro.2022.102181.

References

Abou Ouf, M., 1992. Foraminiferal Distriqution in recent Sediments of Jizan Shelf, Red Sea, Saudi Arabia. J.K.A.U. Mar. Sci. 3, 25–38.
Abou Ouf, M., El Shater, A., 1992. Sedimentology and Mineralogy of Jizan Shelf Sediments Red Sea, Saudi Arabia. J.K.A.U. Mar. Sci. 3, 39–54.
Abu-Zied, R.H., 2013. Effect of the Red Sea brine-filled deeps (Shaban and Kebrit) on the composition and abundance of benthic and planktonic foraminifera. Arab. J. Geosci. 6, 3809–3826. https://doi.org/10.1007/s12517-012-0641-3.
Abu-Zied, R.H., Bantan, R.A., 2013. Hypersaline benthic foraminifera from the Shuaiba Lagoon, eastern Red Sea, Saudi Arabia : their environmental controls and usefulness in sea-level reconstruction. Mar. Micropaleontol. 103, 51–67. https://doi.org/10.1016/j.marmicro.2013.07.005.
Abu-Zied, R., Orif, M.I., 2019. Recent environmental changes of Al-Salam Lagoon as inferred from core sediment geochemistry and benthic foraminifera, Jeddah City, Saudi Arabia. Environ. Earth Sci. 78, 1–12. https://doi.org/10.1007/s12665-019-8057-y.
Abu-Zied, R.H., Rohling, E.J., Jorissen, F.J., Fontanier, C., Casford, J., Cooke, S., 2008. Benthic foraminiferal response to changes in bottom-water oxygenation and organic carbon flux in the eastern Mediterranean during LGM to recent times. Mar. Micropaleontol. 67, 46–68. https://doi.org/10.1016/j.marmicro.2007.08.006.
Abu-Zied, R.H., Bantan, R.A., Basaham, A.S., Mamoney, M., Al-Washmi, H., 2011. Composition, distribution and taphonomy of nearshore benthic foraminifera of the Farasan Islands, southern Red Sea, Saudi Arabia. J. Foraminifer. Res. 41, 349–362.
Almalki, K.A., Bantan, R.A., 2016. Lithologic units and stratigraphy of the Farasan Islands, Southern Red Sea. Carbonates Evaporites 31, 115–128. https://doi.org/10.1007/s13146-015-0247-4.
Al-Mikhlafi, A.S., Hibbert, F.D., Edwards, L.R., Cheng, H., 2021. Holocene relative sea-level changes and coastal evolution along the coastlines of Kamaran Island and As-Salif Peninsula, Yemen, southern Red Sea. Quat. Sci. Rev. 252 https://doi.org/10.1016/j.quascirev.2020.106719.
Almogi-Labin, A., Hemleben, C., Meischner, D., Erlenkeuser, H., 1991. Paleoenvironmental events during the last 13000 years in the Central Red Sea as recorded by pteropoda. Paleoceanography 6, 83–98.
Almogi-Labin, A., Hemleben, C., Meischner, D., Erlenkeuser, H., 1996. Response of Red Sea deep-water agglutinated foraminifera to water-mass changes during the Late Quaternary. Mar. Micropaleontol. 28, 283–297.
Almogi-Labin, A., Schmiedl, G., Hemleben, C., Siman-tov, R., Segl, M., Meischner, D., 2000. The influence of the NE winter monsoon on productivity changes in the Gulf of Aden, NW Arabian Sea, during the last 530 ka as recorded by foraminifera. Mar. Micropaleontol. 40, 295–319.
Alperin, M.I., Cusminsky, G.C., Bernasconi, E., 2011. Benthic foraminiferal morphogroups on the Argentine continental shelf. J. Foraminifer. Res. 41, 155–166. https://doi.org/10.2113/gsjfr.41.2.155.
Anderson, D.M., Prell, W.L., 1992. The structure of the southwest monsoon winds over the Arabian Sea during the late Quaternary: observations, simulations, and marine geologic evidence. J. Geophys. Res. 97, 15481–15487.
Arz, H.W., Patzold, J., Muller, P., 2003. Influence of Northern Hemisphere climate and global sea level rise on the restricted Red Sea marine environment during termination I. Paleoceanography 18, 1053. https://doi.org/10.1029/2002PA000864.
Arz, H.W., Lamy, F., Ganopolski, A., Nowaczyk, N., Patzold, J., 2007. Dominant Northern Hemisphere climate control over millennial-scale glacial sea-level variability. Quat. Sci. Rev. 26, 312–321. https://doi.org/10.1016/j.quascirev.2006.07.016.
Babker, Z., Elagib, N., Al Zayed, I.S., Sulieman, R., 2020. Floodwater harvesting to manage irrigation water and mesquite encroachment in a data-sparse river basin: an eco-hydrological approach. River Res. Appl. 1852–1867 https://doi.org/10.1002/rra.3703.
Badawi, A., 2015. Late quaternary glacial/interglacial cyclicity models of the Red Sea. Environ. Earth Sci. 73, 961–977. https://doi.org/10.1007/s12665-014-3446-8.
Badawi, A., Schmiedl, G., Hemleben, C., 2005. Impact of late Quaternary environmental changes on deep-sea benthic foraminiferal faunas of the Red Sea. Mar. Micropaleontol. 58, 13–30. https://doi.org/10.1016/j.marmicro.2005.08.002.
Bailey, G.N., Deves, M.H., Inglis, R.H., Meredith-williams, M.G., Momber, G., Sakellariou, D., Sinclair, A.G.M., Rousakis, G., Al Ghamdi, S., Alsharekh, A.M., 2015. Blue Arabia: Palaeolithic and underwater survey in SW Saudi Arabia and the role of coasts in Pleistocene dispersals. Quat. Int. 382, 42–57. https://doi.org/10.1016/j.quaint.2015.01.002.
Bailey, G., Meredith-Williams, M.G., Alsharekh, A., Hausmann, N., 2019. The archaeology of Pleistocene coastal environments and human dispersals in the Red Sea: Insights from the Farasan Islands. In: Rasul, N.M.A., Stewart, I.C.F. (Eds.), Geological Setting, Palaeoenvironment and Archaeology of the Red Sea. Springer Cham, pp. 587–608. https://doi.org/10.1007/978-3-319-99408-6_26.
Bantan, R.A., Abu-Zied, R.H., 2014. Sediment characteristics and molluscan fossils of the Farasan Islands shorelines, southern Red Sea, Saudi Arabia. Arab. J. Geosci. 7, 773–787. https://doi.org/10.1007/s12517-013-0851-3.
Barmawidjaja, D.M., Jorissen, F.J., Puskaric, S., Van der Zwaan, G., 1992. Microhabitat selection by benthic foraminifera in the northern Adriatic Sea. J. Foraminifer. Res. 22, 297–317.
Basaham, A.S., 2009. Geochemistry of Jizan shelf sediments, southern Red Sea coast of Saudi Arabia. Arab. J. Geosci. 2, 301–310. https://doi.org/10.1007/s12517-009-0033-5.
Biton, E., Gildor, H., Peltier, W.R., 2008. Red Sea during the last Glacial Maximum : Implications for sea level reconstruction. Paleoceanography 23, 1–12. https://doi.org/10.1029/2007PA001431.
Blott, S.J., Pye, K., 2001. Gradistat: a grain size distribution and statistics package for the analysis of unconsolidated sediments. Earth Surf. Process. Landf. 26, 1237–1248.
Böll, A., Schulz, H., Munz, P., Rixen, T., Gaye, B., Emeis, K., 2015. Contrasting Sea surface temperature of summer and winter monsoon variability in the northern Arabian Sea over the last 25 ka. Palaeogeogr. Palaeoclimatol. Palaeoecol. 426, 10–21. https://doi.org/10.1016/j.palaeo.2015.02.036.
Bunzel, D., Schmiedl, G., Lindhorst, S., Mackensen, A., Reolid, J., Romahn, S., Betzler, C., 2017. A multi-proxy analysis of late Quaternary Ocean and climate variability for the Maldives. Inner Sea. Clim. Past 13, 1791–1813.
Caley, T., Malaizé, B., Zaragosi, S., Rossignol, L., Bourget, J., Eynaud, F., Martinez, P., Giraudeau, J., Charlier, K., Ellouz-zimmermann, N., 2011. New Arabian Sea records help decipher orbital timing of Indo-Asian monsoon. Earth Planet. Sci. Lett. 308, 433–444. https://doi.org/10.1016/j.epsl.2011.06.019.
Clemens, S.C., Prell, W.L., 2003. A 350,000 year summer-monsoon multi-proxy stack from the Owen Ridge, Northern Arabian Sea. Mar. Geol. 201, 35–51. https://doi.org/10.1016/S0025-3227(03)00207-X.
Corliss, B.H., Fois, E., 1990. Morphotype analysis of deep-sea benthic foraminifera from the Northwest Gulf of Mexico. Palaios 5, 589–605.
De Rijk, S., Troelstra, S., Rohling, E.J., 1999a. Modern benthic foraminifera from Mediterranean surface sediments. J. Foraminifer. Res. 29, 93–103.
De Rijk, S., Troelstra, S.R., Rohling, E.J., 1999b. Benthic foraminiferal distribution in the Mediterranean Sea. J. Foraminifer. Res. 29, 93–103.
De Rijk, S., Jorissen, F.J., Rohling, E.J., Troelstra, S., 2000. Organic flux control on bathymetric zonation of Mediterranean benthic foraminifera. Mar. Micropaleontol. 40, 151–166.
Deplazes, G., Lückge, A., Stuut, J.W., Pätzold, J., Kuhlmann, H., Husson, D., Fant, M., Haug, G.H., 2014. Weakening and strengthening of the Indian monsoon during Heinrich events and Dansgaard-Oeschger oscillations. Paleoceanography 29, 99–114. https://doi.org/10.1002/2013PA002509.
Di Bella, L., Pierdomenico, M., Bove, C., Casalbore, D., Ridente, D., 2021. Benthic foraminiferal response to sedimentary processes in a prodeltaic environment: the Gulf of Patti Case Study. Geosciences 11.

Diz, P., Frances, G., Costas, S., Souto, C., Alejo, I., 2004. Distribution of benthic foraminifera in coarse sedimenrs, Ria de Vigo, NW Iberian margin. J. Foraminifer. Res. 34, 258–275. https://doi.org/10.2113/34.4.258.

Dreano, D., Raitsos, D.E., Gittings, J., Krokos, G., Hoteit, I., 2016. The Gulf of Aden intermediate water intrusion regulates the Southern Red Sea Summer phytoplankton blooms. PLoS One 11. https://doi.org/10.1371/journal.pone.0168440.

Duros, P., Jacinto, R.S., Dennielou, B., Schmidt, S., Lamas, R.M., Gautier, E., Roubi, A., Gayet, N., 2017. Deep – Sea Research I Benthic foraminiferal response to sedimentary disturbance in the Capbreton canyon (Bay of Biscay, NE Atlantic). Deep. Res. Part I 120, 61–75. https://doi.org/10.1016/j.dsr.2016.11.012.

Edelman-Furstenberg, Y., Scherbacher, M., Hemleben, C., Almogi-Labin, A., 2001. Deep-sea benthic foraminifera from the Central Red Sea. J. Foraminifer. Res. 31, 48–59.

Edelman-Furstenberg, Y., Almogi-labin, A., Hemleben, C., 2009. Palaeoceanographic evolution of the Central Red Sea during the late Holocene. The Holocene 1, 117–127.

Ellis, J., Anlauf, H., Kürten, S., Lozano-cortés, D., Alsaffar, Z., Jones, B., Carvalho, S., 2017. Cross shelf benthic biodiversity patterns in the Southern Red Sea. Sci. Rep. 7 https://doi.org/10.1038/s41598-017-00507-y.

Fenton, M., Geiselhart, S., Rohling, E.J., Hemleben, C., 2000. Aplanktonic zones in the Red Sea. Mar. Micropaleontol. 40, 277–294.

Fernandes, C.A., Rohling, E.J., Siddall, M., 2006. Absence of post-Miocene Red Sea land bridges: biogeographic implications. J. Biogeogr. 33, 961–966. https://doi.org/10.1111/j.1365-2699.2006.01478.x.

Fersi, W., Bassinot, F., Lezine, A., 2016. Past productivity variations and organic carbon burial in the Gulf of Aden since the Last Glacial Maximum. Quaternaire 27, 213–226. https://doi.org/10.4000/quaternaire.7655.

Folk, R.L., 1974. Petrology of Sedimentary Rocks. Hemphill Publishing Company, Austin, Texas, p. 78703.

Gaye, B., Böll, A., Segschneider, J., Burdanowitz, N., Emeis, K., Ramaswamy, V., Lahajnar, N., Lückge, A., Rixen, T., 2018. Glacial – interglacial changes and Holocene variations in Arabian Sea denitrification. Biogeosciences 15, 507–527.

Gittings, J.A., Raitsos, D.E., Racault, M., Brewin, R.J.W., Pradhan, Y., Sathyendranath, S., Platt, T., 2017. Remote sensing of environment seasonal phytoplankton blooms in the Gulf of Aden revealed by remote sensing. Remote Sens. Environ. 189, 56–66.

Grant, K.M., Rohling, E.J., Ayalon, A., Ramsey, C.B., Satow, C., Roberts, A.P., 2012. Rapid coupling between ice volume and polar temperature over the past 150,000 years. Nature 491, 744–747. https://doi.org/10.1038/nature11593.

Hartman, A., Torfstein, A., Almogi-labin, A., 2020. Climate swings in the northern Red Sea over the last 150, 000 years from ε Nd and Mg / Ca of marine sediments. Quat. Sci. Rev. 231, 106205 https://doi.org/10.1016/j.quascirev.2020.106205.

Herkat, M., Ladjal, A., 2013. Paleobathymetry of foraminiferal assemblages from the Pliocene of the Western Sahel (North-Algeria). Palaeogeogr. Palaeoclimatol. Palaeoecol. 374, 144–163. https://doi.org/10.1016/j.palaeo.2013.01.013.

Hermelin, J.O., Shimmield, G.B., 1990. The importance of the oxygen minimum zone and sediment geochemistry in the distribution of recent benthic foraminifera in the Northwest Indian Ocean. Mar. Geol. 91, 1–29.

Ivanochko, T.S., Ganeshram, R.S., Brummer, G.A., Ganssen, G., Jung, S.J.A., Moreton, S. G., Kroon, D., 2005. Variations in tropical convection as an amplifier of global climate change at the millennial scale. Earth Planet. Sci. Lett. 235, 302–314. https://doi.org/10.1016/j.epsl.2005.04.002.

Jannink, N.T., Zachariasse, W.J., Van Der Zwaan, G.J., 1998. Living (Rose Bengal stained) benthic foraminifera from the Pakistan continental margin (northern Arabian Sea). Deep-Sea Res. 45, 1483–1513.

Jorissen, F.J., De Stigter, H.C., Widmark, J.G.V., 1995. A conceptual model explaining benthic foraminiferal microhabitats. Mar. Micropaleontol. 26, 3–15.

Jorissen, F., Pia, M., Almogi-labin, A., Barras, C., Bergamin, L., Bicchi, E., El, A., Ferraro, L., Mcgann, M., Morigi, C., Romano, E., Sabbatini, A., Schweizer, M., Spezzaferri, S., 2018. Developing Foram-AMBI for biomonitoring in the Mediterranean: Species assignments to ecological categories. Mar. Micropaleontol. 140, 33–45. https://doi.org/10.1016/j.marmicro.2017.12.006.

Kaiho, K., 1994. Benthic foraminiferal dissolved-oxygen index and dissolved-oxygen levels in the modern ocean. Geology 22, 719–722. https://doi.org/10.1130/0091-7613(1994)022<0719.

Lambeck, K., Purcell, A., Flemming, N.C., Vita-finzi, C., Alsharekh, A.M., Bailey, G.N., 2011. Sea level and shoreline reconstructions for the Red Sea: isostatic and tectonic considerations and implications for hominin migration out of Africa. Quat. Sci. Rev. 30, 3542–3574. https://doi.org/10.1016/j.quascirev.2011.08.008.

Lauterbach, S., Anderson, N., Wang, Y., Blanz, T., Larsen, T., Schneider, R.R., 2020. An ~ 130 kyr record of surface water temperature and δ 18O from the northern Bay of Bengal – investigating the linkage between Heinrich events and Weak Monsoon Intervals in Asia An ~ 130 kyr Record of Surface Water Temperature and δ 18 O from the Northern. Paleoceanogr. Paleoclimatol. 35 https://doi.org/10.1029/2019PA003646.

Leuschner, D.C., Sirocko, F., 2000. The low-latitude monsoon climate during Dansgaard - Oeschger cycles and Heinrich Events. Quat. Sci. Rev. 19, 243–254.

Li, W., El-Askary, H., Qurban, M.A., Proestakis, E., Id, E.M., Piechota, T., Manikandan, K. P., 2018. An assessment of atmospheric and meteorological factors regulating red sea phytoplankton growth. Remote Sens. 10 https://doi.org/10.3390/rs10050673.

Locke, S., Thunell, R.C., 1988. Paleoceanographic record of the last glacial/interglacial cycle in the Red Sea and Gulf of Aden. Palaeogeogr. Palaeoclimatol. Palaeoecol. 64, 163–187.

Manheim, F.T., 1974. Red Sea Geochemistry. In: Initial Reports of the Deep Sea Drilling Project, vol. 23. U.S. Government Printing Office, pp. 975–998.

Mazzulo, J., Graham, A.G., 1988. Technical Note 8: Handbook for Shipboard Sedimentologists.

McCreary, J., Kohler, K., Hood, R.R., Olson, D., 1996. A four-component ecosystem model of biological activity in the Arabian Sea. Progr. Ocean. 37, 193–240. https://doi.org/10.1016/S0079-6611(96)00005-5.

McNeill, L.C., Shillington, D.J., Carter, G.D.O., Everest, J.D., Gawthorpe, R.L., Miller, C., Phillips, M.P., Collier, R.E.L., Cvetkoska, A., De Gelder, G., Diz, P., Doan, M., Ford, M., Geraga, M., Gillespie, J., Hemelsdae, R., Herrero-Bervera, E., Ismaiel, M., Janikian, L., Kouli, K., Le Ber, E., Li, S., Maffione, M., Mahoney, C., Machlus, M., Michas, G., Nixon, C.W., Oflaz, S.A., Omale, A., Panagiotopoulos, K., Pechlivanidou, S., Sauer, S., Seguin, J., Sergiou, S., Zakharova, N., Green, S., 2019. High-resolution record reveals climate-driven environmental and sedimentary changes in an active rift. Sci. Rep. 9 https://doi.org/10.1038/s41598-019-40022-w.

Mendes, I., Gonzalez, R., Dias, J.M.A., Lobo, F., Martins, V., 2004. Factors influencing recent benthic foraminifera distribution on the Guadiana shelf (Southwestern Iberia). Mar. Micropaleontol. 51, 171–192. https://doi.org/10.1016/j.marmicro.2003.11.001.

Meyers, P.A., 1994. Preservation of elemental and isotopic source identification of sedimentary organic matter. Chem. Geol. 114, 289–302.

Mitchell, N.C., Ligi, M., Rohling, E.J., 2015. Red Sea isolation history suggested by Plio-Pleistocene seismic reflection sequences. Earth Planet. Sci. Lett. 430, 387–397. https://doi.org/10.1016/j.epsl.2015.08.037.

Morcos, S.A., 1970. Physical and chemical oceanography of the Red Sea. Oceanogr. Mar. Biol. Annu. Rev. 8, 73–202.

Murray, J., 2006. Ecology and Applications of Benthic Foraminifera. Cambridge University Press.

Naidu, P.D., Malmgren, B.A., 1996. A High-resolution record of Late Quaternary upwelling along the Oman Margin, Arabian Sea based on planktonic foraminifera. Paleoceanography 11, 129–140. https://doi.org/10.1029/95PA03198.

Palchan, D., Stein, M., Almogi-Labin, A., Erel, Y., Goldstein, S.L., 2013. Dust transport and synoptic conditions over the Sahara – Arabia deserts during the MIS6 / 5 and 2 / 1 transitions from grain-size, chemical and isotopic properties of Red Sea cores. Earth Planet. Sci. Lett. 382, 125–139. https://doi.org/10.1016/j.epsl.2013.09.013.

Pavlopoulos, K., Koukousioura, O., Triantaphyllou, M., Vandarakis, D., Marion, S., Procé, D., Chondraki, V., Fouache, E., Kapsimalis, V., 2018. Geomorphological changes in the coastal area of Farasan Al-Kabir Island (Saudi Arabia) since mid Holocene based on a multi-proxy approach. Quat. Int. 493, 198–211. https://doi.org/10.1016/j.quaint.2018.06.004.

Pearman, J.K., Sarma, K.S., Jones, Y.V.B., Carvalho, B.H., 2016. Biodiversity patterns of plankton assemblages at the extremes of the Red Sea. FEMS Microbiol. Ecol. 92 https://doi.org/10.1093/femsec/fiw002.

Pearman, J.K., Ellis, J., Irigoien, X., Sarma, Y.V.B., Jones, B.H., Carvalho, S., 2017. Microbial planktonic communities in the Red Sea : high levels of spatial and temporal variability shaped by nutrient availability and turbulence. Sci. Rep. 7 https://doi.org/10.1038/s41598-017-06928-z.

Platon, E., Sen Gupta, B., Rabalais, N., Turner, E., 2005. Effect of seasonal hypoxia on the benthic foraminiferal community of the Louisiana inner continental shelf: The 20th century record. Mar. Micropaleontol. 54, 263–283. https://doi.org/10.1016/j.marmicro.2004.12.004.

Raitsos, D.E., Yi, X., Platt, T., Racault, M., Brewin, R.J.W., Pradhan, Y., Papadopoulos, V. P., Sathyendranath, S., Hoteit, I., 2015. Monsoon oscillations regulate fertility of the Red Sea. Geophys. Res. Lett. 42, 855–862. https://doi.org/10.1002/2014GL062882.

Rasul, N.M.A., Stewart, I.C.F., 2015. The Red Sea - The Formation, Morphology, Oceanography and Environment of a Young Ocean Basin. Springer-Verlag Berlin Heidelberg. https://doi.org/10.1007/978-3-662-45201-1.

Reichart, G.J., Lourens, L.J., Zachariasse, W.J., 1998. Temporal variability in the northern Arabian Sea Oxygen Minimum Zone (OMZ) during the last 225, 000 years. Paleoceanography 13, 607–621.

Roberts, A.P., Rohling, E.J., Grant, K.M., Larrasoaña, J.C., Liu, Q., 2011. Atmospheric dust variability from Arabia and China over the last 500, 000 years. Quat. Sci. Rev. 30, 3537–3541. https://doi.org/10.1016/j.quascirev.2011.09.007.

Rohling, E.J., Zachariasse, W.J., 1996. Red Sea outflow during the last glacial maximum. Quat. Int. 31, 77–83.

Rohling, E.J., Fenton, M., Jorissen, F.J., Bertrand, P., Ganssen, G., P, C.J., 1998. Magnitudes of sea-level lowstands of the past 500,000 years. Nature 394, 162–165.

Sakellariou, D., Rousakis, G., Panagiotopoulos, I., Morfis, I., Bailey, G.N., 2019. Geological structure and late quaternary geomorphological evolution of the Farasan Islands Continental Shelf, South Red Sea, SW Saudi Arabia. In: Rasul, N.M.A., Stewart, I.C.F. (Eds.), Geological Setting, Palaeoenvironment and Archaeology of the Red Sea. Springer Cham, pp. 629–652. https://doi.org/10.1007/978-3-319-99408-6_28.

Sanchez-Goni, M., Harrison, S., 2010. Millennial-scale climate variability and vegetation changes during the last Glacial: Concepts and terminology. Quat. Sci. Rev. 29, 2823–2827. https://doi.org/10.1016/j.quascirev.2009.11.014.

Saraswat, R., Roy, C., Khare, N., Saalim, S.M., Kurtarkar, S.R., 2018. Assessing the environmental significance of benthic foraminiferal morpho-groups from the northern high latitudinal regions. Polar Sci. 18, 28–38. https://doi.org/10.1016/j.polar.2018.08.002.

Schimmelmann, A., Lange, C.B., Schieber, J., Francus, P., Ojala, A.E.K., Zolitschka, B., 2016. Varves in marine sediments : a review. Earth Sci. Rev. 159, 215–246. https://doi.org/10.1016/j.earscirev.2016.04.009.

Schulz, H., Von Rad, U., Erlenkeuser, H., 1998. Correlation between Arabian Sea and Greenland climate oscillations of the past 110,000 years. Nature 393, 54–57.

Schulz, H., Von Rad, U., Ittekkot, V., 2002. Planktic foraminifera, particle flux and oceanic productivity off Pakistan, NE Arabian Sea: modern analogues and application to the palaeoclimatic record. In: Clift, P.D., Kroon, D., Gaedicke, C., Craig (Eds.), The Tectonic and Climatic Evolution of 499 the Arabian Sea Region, pp. 499–516.

Sen Gupta, B.K., 2003. Modern Foraminifera. Kluwer Academic Publishers.
Sen Gupta, B.K., Machain-Castillo, M.L., 1993. Benthic foraminifera in oxygen-poor habitats. Mar. Micropaleontol. 20, 183–201.
Sergiou, S., Geraga, M., Rohling, E.J., Rodríguez-Sanz, L., Hadjisolomou, E., Paraschos, F., Sakellariou, D., Bailey, G., 2022. Influences of sea level changes and the South Asian Monsoon on southern Red Sea oceanography over the last 30 ka. Quat. Res. 1–19 https://doi.org/10.1017/qua.2022.16.
Shakun, J.D., Burns, S.J., Fleitmann, D., Kramers, J., Matter, A., Al-subary, A., 2007. A high-resolution, absolute-dated deglacial speleothem record of Indian Ocean climate from Socotra Island, Yemen. Earth Planet. Sci. Lett. 259, 442–456. https://doi.org/10.1016/j.epsl.2007.05.004.
Siccha, M., Trommer, G., Schulz, H., Hemleben, C., Kucera, M., 2009. Factors controlling the distribution of planktonic foraminifera in the Red Sea and implications for the development of transfer functions. Mar. Micropaleontol. 72, 146–156. https://doi.org/10.1016/j.marmicro.2009.04.002.
Siddall, M., Smeed, D.A., Matthiesen, S., Rohling, E.J., 2002. Modelling the seasonal cycle of the exchange flow in Bab El Mandab (Red Sea). Deep-Sea Res. 49, 1551–1569.
Siddall, M., Rohling, E.J., Almogi-Labin, A., Hemleben, C., Meischner, D., Schmeltzer, I., Smeed, D.A., 2003. Sea-level fluctuations during the last glacial cycle. Nature 423, 853–858. https://doi.org/10.1038/nature01687.1.
Siddall, M., Smeed, D.A., Hemleben, C., Rohling, E.J., Schmelzer, I., Peltier, W.R., 2004. Understanding the Red Sea response to sea level. Earth Planet. Sci. Lett. 225, 421–434. https://doi.org/10.1016/j.epsl.2004.06.008.
Singh, A.D., Jung, S.J.A., Darling, K., Ganeshram, R., Ivanochko, T., Kroon, D., 2011. Productivity collapses in the Arabian Sea during glacial cold phases Productivity collapses in the Arabian Sea during glacial cold phases. Paleoceanography 26. https://doi.org/10.1029/2009PA001923.
Singh, A.D., Rai, A.K., Verma, K., Das, S., Bharti, S.K., 2015. Benthic foraminiferal diversity response to the climate induced changes in the eastern Arabian Sea oxygen minimum zone during the last 30 ka BP. Quat. Int. 374, 118–125. https://doi.org/10.1016/j.quaint.2014.11.052.
Singh, A.K., Tiwari, M., Shrivastava, A., Sinha, D.K., 2016. Wind strength variability in the Western Arabian Sea since the Last Glacial Maximum: Southwest vs. Northeast Monsoon Modes. J. Clim. Chang. 2, 57–70. https://doi.org/10.3233/JCC-160017.
Sofianos, S.S., Johns, W.E., 2007. Observations of the summer Red Sea circulation. J. Geophys. Res. 112 https://doi.org/10.1029/2006JC003886.
Sofianos, S., Johns, W.E., 2015. Water mass formation, overturning circulation, and the exchange of the Red Sea with the Adjacent Basins. In: Rasul, N.M.A., Stewart, I.C.F. (Eds.), The Red Sea the Formation. Morphology, Oceanography and Environment of a Young Ocean Basin, pp. 343–353. https://doi.org/10.1007/978-3-662-45201-1.
Stoffers, P., Ross, D.A., 1974. Sedimentary history of the Red Sea. In: Initial Reports of the Deep Sea Drilling Project, vol. 23. U.S. Government Printing Office, pp. 849–865.
Triantafyllou, G., Yao, F., Petihakis, G., Tsiaras, K.P., Raitsos, D.E., Hoteit, I., 2014. Exploring the Red Sea seasonal ecosystem functioning using a three-dimensional biophysical model. J. Geophys. Res. Ocean. 119, 1791–1811. https://doi.org/10.1002/2013JC009641.
Trommer, G., Siccha, M., Rohling, E.J., Grant, K., Van Der Meer, M.T.J., Schouten, S., Hemleben, C., Kucera, M., 2010. Millennial - scale variability in Red Sea circulation in response to Holocene insolation forcing. Paleoceanography 25, PA3203. https://doi.org/10.1029/2009PA001826.
Trommer, G., Siccha, M., Rohling, E.J., Grant, K., Van Der Meer, M.T.J., Schouten, S., Baranowski, U., Kucera, M., 2011. Sensitivity of Red Sea circulation to sea level and insolation forcing during the last interglacial. Clim. Past 7, 941–955. https://doi.org/10.5194/cp-7-941-2011.
Van der Zwaan, G., Jorissen, F.J., De Stigter, H.C., 1990. The depth dependency of planktonic/benthic foraminiferal ratios: Constraints and applications. Mar. Geol. 95, 1–16.
Van Iperen, J., Helder, W., 1985. A method for the determination of organic carbon in calcareous marine sediments. Mar. Geol. 64, 179–187.
Verma, K., Singh, H., Singh, A.D., Singh, P., Satpathy, R., Naidu, D.P., 2021. Benthic foraminiferal response to the millennial-scale variations in monsoon-driven productivity and deep-water oxygenation in the Western Bay of Bengal during the last 45 ka. Front. Mar. Sci. 8 https://doi.org/10.3389/fmars.2021.733365.
Werner, F., Lange, K., 1975. A bathymetric survey of the sill area between the Red Sea and the Gulf of Aden. Geol. Jahrb. D13, 125–130.
Woelk, S., Quadfasel, D., 1996. Renewal of deep water in the Red Sea during 1982-1987. J. Geophys. Res. 101, 18155–18165.
WoRMS Editorial Board, . World Register of Marine Species. Available from. https://www.marinespecies.org. at VLIZ. Accessed 2021-08-23 [WWW Document]. https://doi.org/10.14284/170.